

## Multiscale Hydro-Thermo-Mechanical Analysis of Hydrating Concrete Structures

L. Jendele<sup>1</sup>, V. Šmilauer<sup>2</sup>, M. Hlobil<sup>2</sup> and J. Červenka<sup>1</sup>

<sup>1</sup>Cervenka Consulting, Prague, Czech Republic

<sup>2</sup>Faculty of Civil Engineering, CTU, Prague, Czech Republic

### Abstract

This paper presents the hydro-thermo-mechanical analysis of reinforced concrete structures applicable to engineering practice. The analysis consists of two steps. Firstly, multiscale moisture and heat transport analyses are carried out, accounting for generated heat and moisture consumption due to concrete hydration. Moisture and temperature fields at all material points are computed. Secondly, these results are imported to a mechanical problem in the form of a staggered solution. The whole model has been implemented in the ATENA software, covering creep and damage effects. The validation shows good crack-width predictions during early age of concrete hardening, taking into account autogeneous shrinkage and creep effects.

**Keywords:** hydro-thermo-mechanical analysis, hydration, heat transport, multiscale model, concrete, affinity model.

## 1 Introduction

Early-age concrete shrinkage accompanied with cracking presents a serious threat to concrete durability [1]. In order to prevent early-age cracking, various precautions have been already proposed and implemented into guidelines and codes [2]. The situation complicates, when dealing with unique structures with a lack of former experience. In such particular case, computer modelling and virtual testing may bring answers to optimal setup in terms of concrete composition, curing, insulation, cooling etc. This paper presents a coupled approach for hydro-thermo-mechanical analysis of hydrating concrete structures, taking into account hydration heat, concrete composition, reinforcement and creep.

A large number of models have been already published to account for hydration heat with a transition to creep and shrinkage of reinforced concrete structures [3], [4], [5], [6]. As creep and shrinkage depends strongly on moisture and temperature,

heat and moisture transport analyses are essential parts of the mechanical creep analyses. Heat/moisture transport analysis was presented and validated in a previous paper [7]. Here, the extension to mechanical part is proposed and validated.

The hydro-thermo-mechanical model implemented in ATENA software [8] is now suited for material and structural engineers. A sensitive concrete composition with its individual constituents is treated in a big detail. The reason lies in a variety of concrete composition concerning cement content, aggregate type, fillers, all of them having effects on released heat during hydration, thermal conductivity and capacity.

The sensitivity to concrete composition is supported by results from international benchmark for control of cracking in R/C structures taking place in the year 2010 and known as the ConCrack. There were 18 participating teams competing in the modelling of two reinforced beams using various software and approaches. The blind stage revealed that maximum concrete core temperature in RG8 experiment was predicted between 48-65°C against measured 55°C. None of competing teams reproduced correctly a dormant period and hydration kinetics strongly deviated. Results from the mechanical part revealed rather poor performance of mechanical models and/or inappropriate assumptions in boundary conditions.

## 2 Heat and moisture transport analyses

Heat and moisture transport analysis is the first part of the full hydro-thermo-mechanical solution presented in this paper and its objective is to calculate heat and moisture fields (at each material point of the structure). These are automatically transferred into the subsequent mechanical analysis and used for:

- Accuracy improvement of creep prediction models (in the case of long-term analysis).
- Calculation for temperature related loads, such as thermal expansion and contraction.
- Inclusion of the effect of elevated temperature over 100°C on the material behaviour under fire, such as spalling.

The models used for heat/moisture analysis are described in the next respective sections.

### 2.1 Heat transport

Fourier law is used to calculate heat transport in the structure. The corresponding governing equation reads

$$\frac{\partial}{\partial t}(Q) = -div(\underline{q}_T) \quad (1)$$

where  $Q$  is the total amount of heat accumulated in a unit volume, [J/m<sup>3</sup>].  $Q$  can be decomposed to

$$Q = Q_0 + \int \frac{\partial Q}{\partial T} dT + Q_h \quad (2)$$

$$\frac{\partial Q}{\partial t} = \frac{\partial Q}{\partial T} \frac{\partial T}{\partial t} + \frac{\partial Q_h}{\partial t} = C_T \frac{\partial T}{\partial t} + \frac{\partial Q_h}{\partial t}$$

where  $C_T$  is heat capacity [J/(K.m<sup>3</sup>)],  $Q_h$  is total hydration heat at time  $t$ , [J/m<sup>3</sup>] and  $q_T$  is heat flux [J/(s.m<sup>2</sup>)]. Heat flux  $q_T$  is calculated using

$$q_T = -\Lambda \nabla(T) \quad (3)$$

$\Lambda$  stands for tensor of heat conductivities, e.g. [J/(s.m.K)] and  $T$  is temperature, [°C].

### 2.1.1 Hydration heat

The analysis is based on the calibrated affinity hydration model [7]. It accounts for all stages of cement hydration and calculates the rate of degree of hydration  $\alpha$ ,  $\alpha \in \langle 0 \dots 1 \rangle$ . The model utilizes chemical affinity  $\tilde{A} = \tilde{A}(\alpha)$ , [s<sup>-1</sup>], which is determined for an isothermal temperature 25°C

$$\frac{\partial \alpha}{\partial t} = \tilde{A}_{25} \exp \left[ \frac{E_a}{R} \left( \frac{1}{T_{25}} - \frac{1}{T} \right) \right] \quad (4)$$

where  $R$  is gas constant  $8314.41 \frac{\text{J}}{\text{kmol K}}$ ,  $T$  is current temperature [K],  $T_{25}$  is a reference temperature [K], and the activation energy  $E_a$  is approximately 40 kJ/mol. Having history of  $\alpha$ , the hydration heat released from a unit cement is calculated as

$$\frac{Q_h}{Q_{h,pot}} \approx \alpha \quad (5)$$

$$\frac{1}{Q_{h,pot}} \frac{\partial Q_h}{\partial t} = \frac{\partial \alpha}{\partial t} = \tilde{A}_{25} \exp \left[ \frac{E_a}{R} \left( \frac{1}{T_{25}} - \frac{1}{T} \right) \right] \quad (6)$$

where  $Q_{h,pot}$  is potential hydration heat, [J/kg]. Concrete is treated as a five-component medium, composed from cement, water, aggregates, filler and air. Scaling of hydration heat to the concrete occurs from a known composition. Each component carries information about its capacity and conductivity.

### 2.1.2 Heat capacity

Heat capacity of concrete is computed by proportional summation of the present constituents in the concrete mixture. The components' contribution coefficients are their volumetric fractions, i.e.  $f_{aggregate}$ ,  $f_{filler}$  and  $f_{paste} = f_{water} + f_{cement}$ .

$$C_{concrete} = f_{aggregate} C_{aggregate} + f_{filler} C_{filler} + \hat{C}_{paste} \quad (7)$$

where  $C_{concrete}$ ,  $C_{aggregate}$ ,  $C_{filler}$  and  $\hat{C}_{paste}$  stand for concrete, aggregate, filler and paste capacity (per unit volume). The last term,  $C_{paste}$ , depends also on the degree of hydration  $\alpha$  and is calculated by

$$\hat{C}_{paste} = (f_{cement} C_{cement} + f_{water} C_{water})(1 - 0.26(1 - \exp(-2.9\alpha))) \quad (8)$$

where  $C_{cement}$  is cement capacity at time zero [9].

### 2.1.3 Heat conductivity

The thermal conductivity of concrete is calculated via homogenization principles. Consider conductivity of cement paste  $\lambda_{paste}$  and aggregates  $\lambda_{aggregate}$  such that  $\lambda_{paste} \leq \lambda_{aggregate}$ . The corresponding volume fractions are  $f_{paste}$ ,  $f_{aggregate}$ . The Hashin-Shtrikman lower  $\lambda_{concrete,low}$  and upper bounds  $\lambda_{concrete,upper}$  reads [9]

$$\lambda_{concrete,low,\infty} = \lambda_{paste} + \frac{3f_{aggregate}\lambda_{paste}(\lambda_{aggregate} - \lambda_{paste})}{3\lambda_{paste} + f_{paste}(\lambda_{aggregate} - \lambda_{paste})} \quad (9)$$

$$\lambda_{concrete,upper,\infty} = \lambda_{aggregate} + \frac{3f_{paste}\lambda_{aggregate}(\lambda_{paste} - \lambda_{aggregate})}{3\lambda_{aggregate} + f_{aggregate}(\lambda_{paste} - \lambda_{aggregate})}$$

The chain approach delivers conductivities at four scales in the following order:

1. Homogenize phases cement and water to obtain cement paste. Use average of  $\lambda_{low,\infty}$ ,  $\lambda_{upper,\infty}$  [9].
2. Homogenize cement paste and filler. Use average of  $\lambda_{low,\infty}$ ,  $\lambda_{upper,\infty}$ .
3. Homogenize the latter with air. Use maximum of  $\lambda_{low,\infty}$ ,  $\lambda_{upper,\infty}$ , which corresponds to Mori-Tanaka scheme with air as an inclusion.
4. Homogenize the latter with aggregates to arrive on concrete scale. Use average of  $\lambda_{low,\infty}$ ,  $\lambda_{upper,\infty}$ .

The concrete conductivity at time  $t$  is calculated as:

$$\lambda_{concrete} = \lambda_{concrete,0}(1.0 - 0.248\alpha) \quad (10)$$

where  $\lambda_{concrete,0}$  is the conductivity of fresh concrete obtained from the four-step homogenization.

## 2.2 Moisture transport

The presented model makes no difference between water and water vapour in terms of mass. The governing equations for transport per unit volume reads

$$\frac{\partial w}{\partial t} + \frac{\partial w_h}{\partial t} = -\text{div}(\underline{q}_h) \quad (11)$$

$$C_h \frac{\partial h}{\partial t} + \frac{\partial w_h}{\partial t} = -\text{div}(\underline{q}_h)$$

where  $w$  is moisture content at current time  $t$ , [ $\text{kg}/\text{m}^3$ ],  $w_h$  stands for the amounts of moisture consumed by hydration, [ $\text{kg}/\text{m}^3$ ],  $\underline{q}_h$  is moisture flux, [ $\text{kg} / (\text{m}^2 \text{ s})$ ].  $t$  represents time, [s] and  $h$  relative humidity. The moisture flux is computed by

$$\underline{q}_h = -\mathbf{D}_h \nabla h \quad (12)$$

where  $\nabla h$  is a gradient of relative humidity

### 2.2.1 Moisture consumption due to hydration

Experiments show that 1 kg of cement consumes approximately about 0.23 kg of water when hydrating completely, i.e. typically  $Q_{w,pot}=0.23 \text{ kg/kg}$  Assuming a linear dependence between water consumption  $w^h$  and degree of cement hydration, the water sink term yields:

$$C_{h,t} = \frac{\partial w_h}{\partial t} = \frac{\partial w_h}{\partial \alpha} \frac{\partial \alpha}{\partial t} \quad (13)$$

$$w_h = Q_{w,pot} c \alpha \quad (14)$$

where  $c$  stands for the mass of cement in  $1\text{m}^3$  of concrete.

### 2.2.2 Moisture capacity

A simple constitutive law based on Kuenzel [10] is used to calculate moisture capacity of concrete, see Equation (15). It has two material constants, namely the free water saturation  $w_f$ , [ $\text{kgm}^{-3}$ ], and a dimensionless approximation factor  $b$ . The Moisture content in a unit volume  $w$ , [ $\text{kgm}^{-3}$ ], is:

$$w = w_f \frac{(b-1)h}{b-h} \quad (15)$$

The parameter  $b$  can be determined from the water content  $w_{80}$  at relative humidity  $h = 0.8$

$$b = \frac{h(w_f - w_{80})}{w_f h - w_{80}} \quad (16)$$

The moisture capacity  $C$ , [ $\text{kgm}^{-3}$ ] is calculated as a derivative of moisture content with respect to  $h$

$$C_h = \frac{\partial w}{\partial h} = \frac{w_f (b-1)b}{(b-h)^2} \quad (17)$$

Although the model is fairly, it provides reasonable accuracy.

### 2.2.3 Moisture diffusion

Moisture diffusion is calculated as the sum of water diffusion  $D_h^w$  and water vapour diffusion  $D_h^{vw}$ . The present model accounts for diffusivity mechanism of moisture transport. It is valid for a dense concrete, which has mutually unconnected pores hence the moisture conduction through pores (being driven by water pressure) can be neglected

$$D_h = D_h^w + D_h^{vw} \quad (18)$$

The detail for the calculation of  $D_h$ ,  $\left[ \frac{kg}{ms} \right]$  are present elsewhere [7].

## 3 Mechanical analysis

Mechanical analysis complements the presented hydro-thermal solution. The quasi-static formulation accounts for time related phenomena such as creep and shrinkage in hardening concrete. The presented model is suitable for solutions of reinforced concrete structures with large displacements and large rotations.

The crucial feature of the developed model is to separate short-term and long-term material behaviour. The short-term model captures material response, such as concrete fracture, while the long-term model delivers concrete creep. Parameters for the short-time model are time adjusted, which is the job of the long-term material model.

The coupling between heat/moisture analysis and mechanical analysis occurs via integration points. The meshes for both problems can be different and the data transition happens via isoparametric interpolation.

### 3.1 Long-term material model

Time effects on concrete behaviour in the long-term material model are incorporated via Stieltjes integral [11],

$$\varepsilon(t) = \int_{t'}^t \Phi(t, t') d\sigma + \varepsilon^0(t), \quad (19)$$

where  $\sigma(t)$  = stress in time  $t$ ,  $d\sigma$  = stress increment,  $\varepsilon^0(t)$  = material swelling/shrinkage at time  $t$ , (it accounts for shrinkage/expansion due to temperature change and autogenous shrinkage),  $\Phi(t, t')$  = compliance function of concrete creep,  $t$  = time at observation and  $t'$  = time at loading.

The assumption of linear creep limits the use to cases, where (in long-term time span) structural compression stresses do not exceed about 60% of the concrete strength in compression. However, as creep analysis is typically carried out for structural serviceability conditions, this limitation typically does not pose a problem. Equation (19) is integrated (in time) by Step-by-step method (SBS), in which original material compliance function is replaced by Dirichlet series [12, 13]. Having known stress and strain at the beginning of the time step  $\Delta t$ , i.e. at time  $t$ , the values at the end the step. i.e. at time  $t + \Delta t$  are calculated as follows, see [13],

$$\Delta \bar{\sigma}_t = \tilde{\mathbf{E}}_t (\Delta \bar{\varepsilon}_t - \Delta \tilde{\bar{\varepsilon}}_t) \quad (1.20)$$

$$\bar{\varepsilon}_{t+\Delta t} = \bar{\varepsilon}_t + \Delta \bar{\varepsilon}_t \quad (1.21)$$

$$\bar{\sigma}_{t+\Delta t} = \bar{\sigma}_t + \Delta \bar{\sigma}_t \quad (1.22)$$

where  $\Delta \bar{\sigma}_{t+\Delta t}$  and  $\bar{\varepsilon}_{t+\Delta t}$  are the total stress and the total strain at the time  $t + \Delta t$ .  $\tilde{\mathbf{E}}_t$  is time adjusted material rigidity matrix and  $\Delta \tilde{\bar{\varepsilon}}_t$  is vector of artificial strains to simulate the effect of creep in the material. Any model for creep and shrinkage prediction can be used for this type of analysis, e.g. B3 model [14]. It follows from the fact that SBS carries out temporal integration numerically.

Creep and shrinkage behaviour of concrete depends on current humidity and temperature conditions. Hence, before the static analysis we must carry out the moisture and humidity analysis and calculate temperature and humidity histories (at each material point of the structure). This concept corresponds to the staggered solution scheme. The effect of the variable temperature  $T(t)$  is projected to the creep prediction model by using so-called equivalent time values  $t_e(T, t)$ . If the creep prediction material law is calibrated for constant reference temperature  $T_{ref}$ , then for the varying temperature conditions  $T(t)$ , the accurate results are obtained by replacement of all real times  $t$  by the equivalent times  $t_e$ . The equivalent times are defined e.g. in Section 1.7.2 in [14].

Each structural material point has its distinct temperature history and hence distinct creep prediction material parameters. However, as the differences between temperature histories (and thus in calculation  $t_e$ ) of neighbouring material points are often small, it suffices to use only a couple of "master" or "average" temperature histories. The original material point history is then replaced by the closest master history. This approach significantly reduces number of required material parameters sets.

### 3.2 The short-term material model

The short-term material model accounts for all nonlinear behaviour due to crack developments, material hardening and softening etc. Its prediction heavily depends on current stress-strain conditions in each material point and possibly also on its history. The variable parameters, mainly Young's modulus, initial strains, compressive and tensile strengths etc. are at a particular time computed by the linear creep model described above.

The short-term concrete mechanical model follows the original theory in [15]. The material model formulation is based on the strain decomposition into elastic  $\varepsilon_{ij}^e$ , plastic  $\varepsilon_{ij}^p$  and fracturing  $\varepsilon_{ij}^f$  components [16].

$$\varepsilon_{ij} = \varepsilon_{ij}^e + \varepsilon_{ij}^p + \varepsilon_{ij}^f \quad (23)$$

The new stress state is then computed by the formula:

$$\sigma_{ij}^n = \sigma_{ij}^{n-1} + E_{ijkl} (\Delta \varepsilon_{kl} - \Delta \varepsilon_{kl}^p - \Delta \varepsilon_{kl}^f) \quad (24)$$

Tensile behaviour of concrete is modelled by non-linear fracture mechanics with a simple Rankine-based criterion.

$$F_i^f = \sigma_i'' - f_{ti}'(w_i') \leq 0 \quad (25)$$

A smeared crack concept is adopted with the following parameters: tensile strength  $f_t$ , shape of the stress-crack opening curve  $f_t(w)$  and fracture energy  $G_F$ . It is assumed that strains and stresses are converted into the material directions, which in a case of rotated crack model correspond to the principal stress directions, and in a case of a fixed crack model to the principal directions at the onset of cracking. Therefore,  $\sigma_i''$  identifies the trial stress and  $f_{ti}'$  tensile strength in the material direction  $i$ . The prime symbol denotes quantities in the material directions. This approach is combined with the crack band method of Bažant and Oh [17]. In this formulation, the cracking strain is related to the element size. Consequently, the softening law in terms of strains for the smeared model is calculated for each element individually, while the crack-opening law is preserved. The model uses an exponential softening law of Hordijk [18].

The compressive behaviour is modelled using a plasticity-based model with failure surface defined by the three-parameter criterion form [19]

$$F_{3p}^p = \left[ \sqrt{1.5} \frac{\rho}{f_c} \right]^2 + m \left[ \frac{\rho}{\sqrt{6} f_c} r(\theta, e) + \frac{\xi}{\sqrt{3} f_c} \right] - c = 0 \quad (26)$$

where

$$m = 3 \frac{f_c^2 - f_t^2}{f_c f_t} \frac{e}{e+1}$$

$$r(\theta, e) = \frac{4(1-e^2) \cos^2 \theta + (2e-1)^2}{2(1-e^2) \cos \theta + (2e-1) \left[ 4(1-e^2) \cos^2 \theta + 5e^2 - 4e \right]^{\frac{1}{2}}} \quad (27)$$

In the above equations,  $(\xi, \rho, \theta)$  are Heigh-Vestergaard coordinates, and  $f_c$  and  $f_t$  are compressive strength and tensile strength respectively. Parameter  $e \in \langle 0.5, 1.0 \rangle$  defines the roundness of the failure surface.

The surface evolves during the yielding/crushing process by the hardening/softening laws based on equivalent plastic strain defined as

$$\Delta \varepsilon_{eq}^p = \min(\Delta \varepsilon_i^p) \quad (28)$$

Hardening  $\varepsilon_{eq}^p \in \langle -\varepsilon_c^p; 0 \rangle$ :

$$f_c(\varepsilon_{eq}^p) = f_{co} + (f_c - f_{co}) \sqrt{1 - \left( \frac{\varepsilon_c^p - \varepsilon_{eq}^p}{\varepsilon_c^p} \right)^2} \quad (29)$$

Softening  $\varepsilon_{eq}^p \in \langle -\infty; -\varepsilon_c^p \rangle$ :

$$\begin{aligned} c &= \left( 1 - \frac{w_c}{w_d} \right)^2, \quad w_c \in \langle -w_d; 0 \rangle \\ c &= 0, \quad w_c \in \langle -\infty; w_d \rangle \\ w_c &= (\varepsilon_{eq}^p - \varepsilon_c^p) L_c \end{aligned} \quad (30)$$

When concrete crushing enters into the softening regime, an analogous approach to the crack band model is used also for the localization in compression within the crushing band  $L_c$ . A direct return-mapping algorithm is used to solve the predictor-corrector equation of the plasticity model.

$$F^p(\sigma_{ij}^t - \sigma_{ij}^p) = F^p(\sigma_{ij}^t - \Delta\lambda l_{ij}) = 0 \quad (31)$$

The plastic stress  $\sigma_{ij}^p$  is a product of plastic multiplier  $\Delta\lambda$  and the return direction  $l_{ij}$ , which is defined as follows

$$l_{ij} = E_{ijkl} \frac{\partial G^p(\sigma_{kl}^t)}{\partial \sigma_{kl}} \quad (32)$$

$$\Delta\varepsilon_{ij}^p = \Delta\lambda \frac{\partial G^p(\sigma_{ij}^t)}{\partial \sigma_{ij}} \quad (33)$$

The plastic potential  $G^p$  is given by

$$G^p(\sigma_{ij}) = \beta \frac{1}{\sqrt{3}} I_1 + \sqrt{2J_2} \quad (34)$$

where  $\beta$  determines the return direction. If  $\beta < 0$ , material is being compacted during crushing, if  $\beta = 0$ , the material volume is preserved, and if  $\beta > 0$ , the material is dilating.

A special iterative algorithm analogous to multi-surface plasticity is used to solve the plastic and fracture models such that the final stress tensors in both models are identical. This algorithm is schematically shown in two-dimensions in Figure 1.

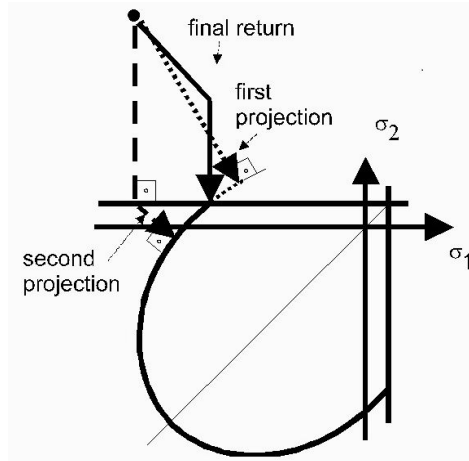


Figure 1: Iterative algorithm for solving interaction of fracture-plastic surfaces.

The presented model is aimed to calculate primarily reinforced concrete structures. In such particular case, two material laws are used; the above described model for adjacent concrete and a 1D model for reinforcement. The latter model can be any time-independent model, such a multilinear 1D model, elastoplastic model with hardening etc.

## 4 Validation

Validation of the coupled hydro-thermo-hydro-mechanical analysis is based on a well-documented ConCrack benchmark experiment RG8. For further information see <http://www.concrack.org/>. 18 teams had modelled the beam RG8 and their results were gathered by the organizer during a blind stage. In the next feedback stage, the teams received their experimental data with the simulations.

Figure 2 shows the overall geometry of the beam RG8 with two massive heads on both sides and two restraining steel struts. The central beam part has dimensions 0.5x0.8x5.1 m and is reinforced. The benchmark experiment provides data on cement mineral composition, cement fineness, concrete composition, reinforcement, geometry, external temperature, internal temperature in three points, adiabatic concrete temperature and displacements of two points C,D located on the beam axis 2.5 m apart.

In order to succeed in the coupled simulation, hydration models had to be validated. Adiabatic experiment showed that CEMHYD3D hydration model predicts correct temperature rise, calibrating only the length of dormant period. The four-parametric affinity model has been calibrated afterwards [7]. Parameters of the affinity model are  $B_1=1.8 \text{ h}^{-1}$ ,  $B_2=1.0e-5$ ,  $\eta=7.0$ ,  $\text{DoH}_\infty = 0.90$ . Figure 4 demonstrates that both models approximated reasonably well experimental data, especially at younger ages. It reveals evident negative slope that documents energy loss in the adiabatic experiment.



Figure 2: A validated massive beam RG8 with restrained shrinkage (image and data from the database Cheops).

The same model was used for heat/moisture transport and mechanical parts. It is shown in Figure 3. Note that the heads were reduced and the struts tied directly to the surfaces of the central beam.

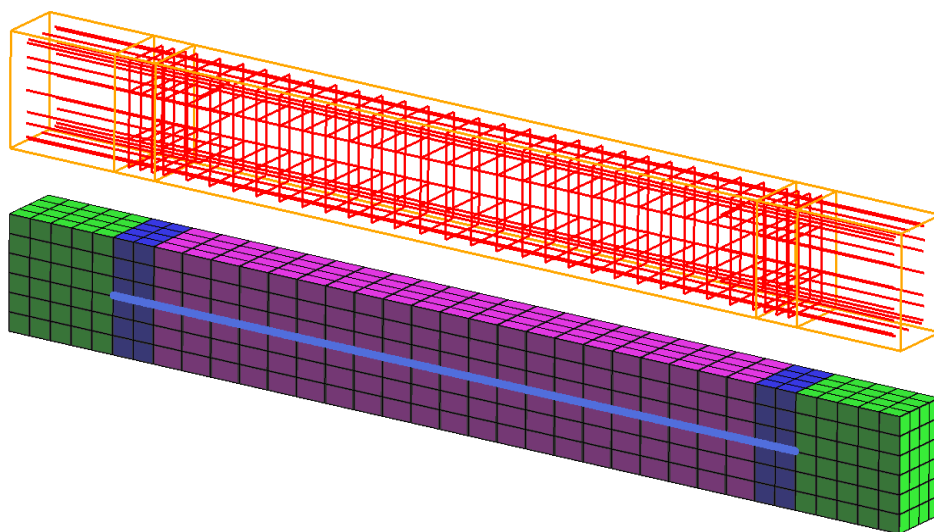


Figure 3: Our model showing the reinforcement and material assignment.

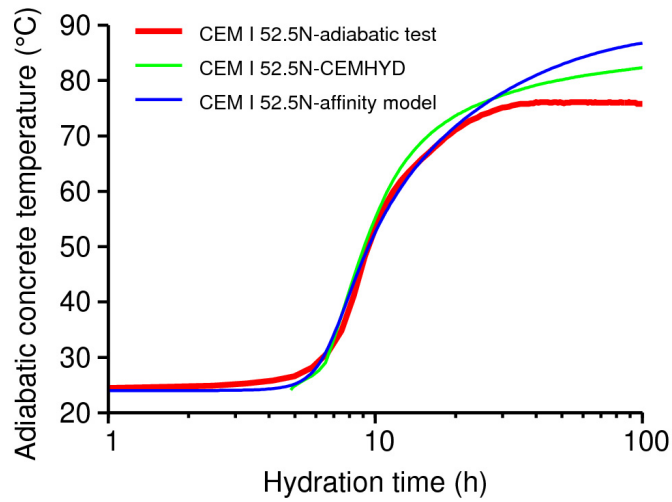
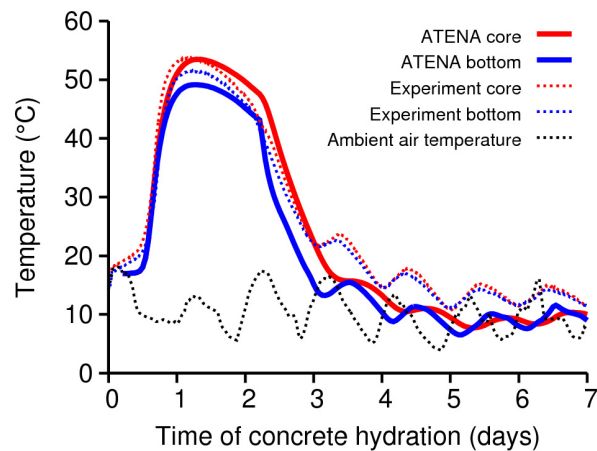


Figure 4: Validation of CEMHYD3D model and the affinity model in concrete adiabatic test.

Pilot calculation revealed clinker content in the cement CEM I had to be lower than declared. The middle beam was thermally insulated by a layer above 200 mm of expanded polystyrene since the casting. From the chemical composition, the potential energy of the clinker is 498 J/g of cement. The original concrete composition stated 400 kg/m<sup>3</sup> of cement, which would lead to temperatures exceeding 70°C as in the adiabatic experiment. In reality, maximum measured temperature was only 53.7°C at 30 hours of hydration. For this reason, we decided to reduce the cement content to 320 kg/m<sup>3</sup>. Figure 5 validates temperatures in the bottom sensor located 50 mm above the surface and in the core of the beam. After two days of hydration the expanded polystyrene was stripped off and the beam surface was exposed to ambient air temperature. The experimental temperatures are a bit higher, probably due to additional supply of solar energy which was ignored in the model. After approximately 4 days, the beam temperatures follow the ambient air fluctuations. The relative humidity drops to 0.88 uniformly in the cross section (without a validation data).



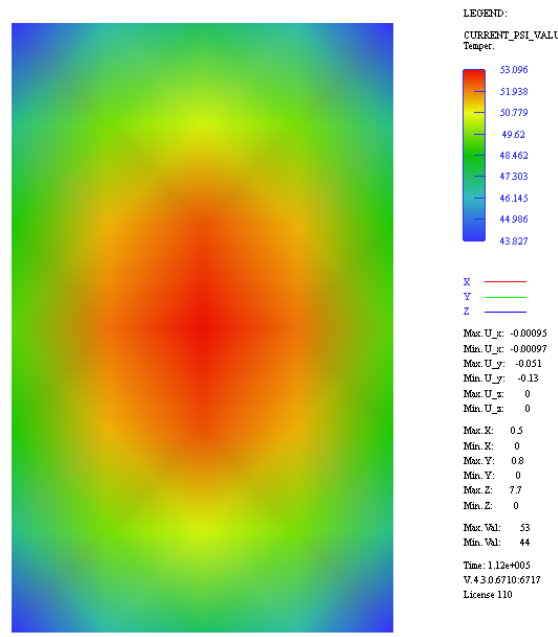


Figure 5: Validation of core and bottom temperature. The bottom subfigure shows the temperature field at the maximum temperature at 30 hours.

The mechanical part uses standard parameters of ATENA concrete C50/60. The computation runs from 0.1 day to prevent singularity in material parameters in the B3 creep model. Integration time is 2 hours. Five concrete parameters evolve with time. They are listed in the following table including their values at 28days.

<b>Mechanical parameter at 28 days</b>	<b>Value</b>
Cylindrical compressive strength	50 MPa
Young's modulus	37 GPa
Compressive stress at the onset of cracking	4.1 MPa
Tensile strength	1.93 MPa
Fracture energy	48.3 J/m <sup>2</sup>

Table 1: Mechanical time adjusted parameters for concrete C50/60, w/c=0.475.

Autogeneous shrinkage was calibrated from the measured data and does not play a significant role in this concrete with w/c=0.475. Actual humidity is passed to drying shrinkage function which follows the evolution given by B3 model [14].

For the sake of simplicity our model did not consider wings to which the struts are attached, see Figure 3. This was done in order to avoid complexity with additional reinforcement and transverse pre-stressed tendons in the heads. The wings add to the compliance of struts, which is a sensitive factor in the model. Compliance of one strut is about 0.777 mm/MN. Considering wings at the time 0.6 day leads to Young's modulus of 5 GPa. When the wing is treated as a cantilever beam with the length of 0.5 m, the shear and bending compliance give 1.143 mm/MN. Therefore,

the bracing effect of the struts and wings is maintained by reducing the cross-section area of the struts to 25%.

Figure 6 demonstrates the effect of strut bracing. The measure points C,D are 2.5 m apart located on the beam axis. The stiffness reduction has effect up to 3 days of hydration. Afterwards, the displacement of points C,D is controlled by fluctuating temperature of ambient air, straining the struts.

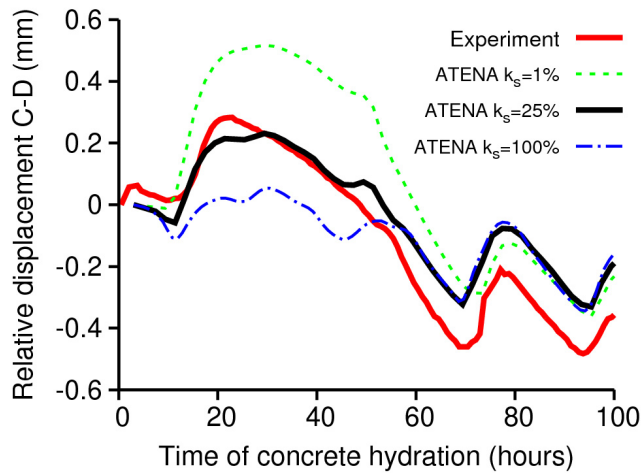
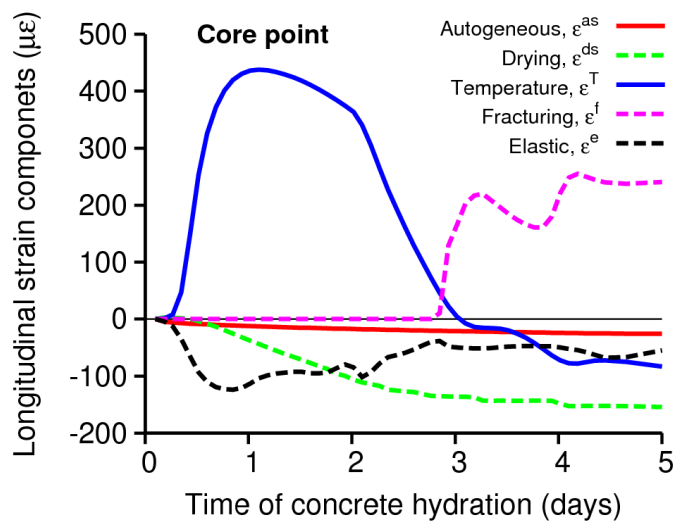


Figure 6: Validation of relative displacements of points C-D with mutual distance 2.5 m on the beam axis. The coefficient  $k_s$  shows stiffness reduction of the struts.

Figure 7 compares strains during concrete hardening. When the sum of strains is positive, the concrete is under tension and fracturing strain is introduced. No plastic strain was found in the calculation, which means no concrete irreversible damage under compression took place. Note that temperature strain is the most effective at early ages and there is no plastic strain.



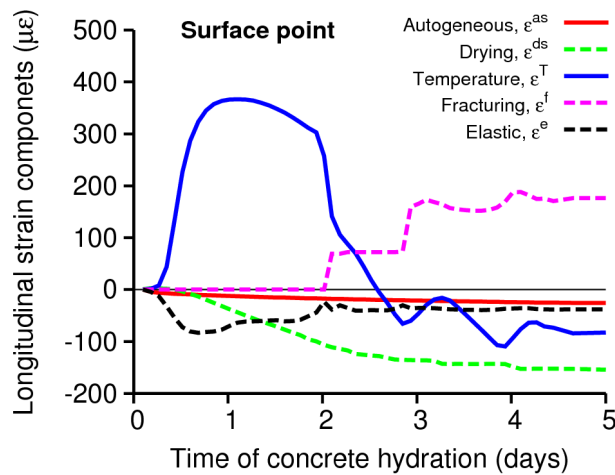


Figure 7: Strain components in the core and surface point of the beam during hardening.

## 5 Conclusion

The performance of presented chemo-thermo-hydro-mechanical model was demonstrated on a hydrating and restrained concrete beam. The whole computation took about 45 minutes on a regular PC. Boundary conditions are critical parts in early ages and temperature effects were found dominating material response under constrained kinematic conditions. Although the task may seem biased with dozens of parameters, default material properties worked reasonably well in the simulation. Further refinement is possible provided more experimental data are available for calibration.

## Acknowledgements

The presented work was carried out within the project FR-TI1/612 from the Ministry of Industry and Trade of the Czech Republic and the grant GAP105/10/2400 from the Czech Science Foundation.

## References

- [1] M. Nilsson, "Thermal Cracking of Young Concrete. Partial Coefficients, Restraint Effects and Influence of Casting Joints", Thesis, Lulea, Sweden, Lulea University of Technology, , 2000.
- [2] A.M. Neville, "Properties of Concrete": John Wiley & Sons, Inc.,1997.
- [3] D. Gawin, F. Pesavento, and B.A. Schrefler, "Hygro-thermo-chemomechanical Modelling of Concrete at Early Ages and Beyond. Part I:

- Hydration and Hygro-thermal Phenomena", *Int. Journal for Numerical Methods in Eng.*, 67(3), 299-331, 2006.
- [4] R. Faria, M. Azenha, and J.A. Figueiras, "Modelling of Concrete at Early Ages: Application to an Externally Restrained Slab", *Cement and Concrete Composites*, 28(6), 572-578, 2006.
- [5] M. Cervera, J. Oliver, and T. Prato, "Thermo-chemo-mechanical Model for Concrete. I: Hydration and Aging", *Jour. Eng. Mech. ASCE*, 125(9), 1018-1027, 1999.
- [6] C. Hellmich, H.A. Mang, and F.J. Ulm, "Hybrid Method for Quantification of Stress States in Shotcrete Tunnel Shells: Combination of 3D in situ Displacement Measurements and Thermochemoplastic Material Law", *Computer and Structures*, 79(2103 – 2115), 2001.
- [7] L. Jendele, V. Šmilauer, J. Cervenka, "Multi-scale Analysis of Heat Transport in Hydrating Concrete Structures", in B.H.V. Topping, Y. Tsompanakis, (Editors), "Proceedings of the Thirteenth International Conference on Civil, Structural and Environmental Engineering Computing", Civil-Comp Press, Stirlingshire, UK, Paper 124, 2011. doi:10.4203/ccp.96.124
- [8] V. Cervenka, J. Cervenka, and L. Jendele, "Atena Program Documentation, Part 1-7", Prague: Cervenka Consl., 2000-2007.
- [9] D.P. Bentz, "Transient Plane Source Measurements of the Thermal Properties of Hydrating Cement Pastes", *Materials and Structures*, 40(10), 1073-1080, 2007.
- [10] H.M. Kuenzel, Simultaneous Heat and Moisture Transport in Building Components. 1D and 2D calculation using simple parameters. Fraunhofer Inst. of Building Physics: Stuttgart1995.
- [11] Z.P. Bazant, "Mathematical Modeling of Creep and Shrinkage of Concrete", New York: John Wiley & Sons, 1988.
- [12] Z.P. Bazant, "Prediction of Concrete Creep Effects Using Age-Adjusted Effective Modulus Method", *ACI Journal*, 69 (4), 212-217, 1972.
- [13] L. Jendele and D.V. Phillips, "Finite Element Software for Creep and Shrinkage in Concrete", *Computer and Structures*, 45 (1), 113-126, 1992.
- [14] Z.P. Bazant and S. Baweja, eds. Creep and Shrinkage Prediction Model for Analysis and design of Concrete Structures: Model B3. Creep and Shrinkage of Concrete, ed. A. Al-Manaseer, ACI Special Publicatino, 1999.
- [15] J. Cervenka and V. Papanikolaou, "Three Dimensional Combined Fracture-Plastic Material Model for Concrete", *Int. Journal of Plasticity*, 24(12), 2192-2220, 2008.
- [16] R. De Borst, "Non-linear analysis of frictional materials", Thesis, Delft, Delft University of Technology, 1986.
- [17] Z.P. Bazant and B.H. Oh, "Crack Band Theory for Fracture of Concrete", *Material and Structures*, 16, 155-177, 1983.
- [18] D.D. Hordijk, "Local Approach to Fatigue of Concrete", Thesis, Delft, Delft University of Technology, 1991.
- [19] P. Menetrey and K.J. Willam, "Triaxial Failure Criterion for Concrete and its Generalization", *ACI Structural Journal*, 92(3), 311-318, 1995.